Applied Geochemistry 180 (2025) 106290

Contents lists available at ScienceDirect

Applied Geochemistry

journal homepage: www.elsevier.com/locate/apgeochem

Thermodynamic description of the Ni(II)-citrate system in alkaline, dilute to concentrated NaCl solutions. Formation of quaternary complexes with ca

O. Almendros-Ginestà [a,*], S. Duckworth [b], P.Q. Fürst [b], T. Missana [a], M. Altmaier [b], X. Gaona [b,**]

[a] CIEMAT, Physical chemistry of actinides and fission products Unit, Madrid, Spain
[b] Karlsruhe Institute of Technology, Institute for Nuclear Waste Disposal, Germany

ARTICLE INFO

Editorial handling by:Gilles Montavon

Keywords:
Nickel
Citrate
Solubility
Calcium
Thermodynamics
Ternary
Quaternary complexes
Cement

ABSTRACT

The impact of citrate (cit) on the solubility of Ni(II) was comprehensively investigated in alkaline 0.1–3.0 M NaCl–NaOH–Na_3cit solutions in the absence and presence of 0.02 mol dm^{-3} $CaCl_2$. Experiments were conducted at a temperature of (22 ± 2)°C under inert gas (Ar) atmosphere. Thermodynamic equilibrium was approached from undersaturation conditions using β-$Ni(OH)_2$(cr).

The characterization by X-ray diffraction of selected solid phases after completing the solubility experiments (~360 days, depending upon experimental series) confirmed that β–$Ni(OH)_2$(cr) controls the solubility of Ni(II) in all investigated systems, both in the absence and presence of Ca. In Ca-free systems, the observed increase in the solubility of Ni(II) is attributed to the formation of binary and ternary Ni(II)–OH–cit aqueous complexes. The use of thermodynamic data currently selected within the Thermochemical Database project of the Nuclear Energy Agency (NEA-TDB) clearly underestimates the solubility of Ni(II) in the hyperalkaline pH_m regime of relevance in cementitious systems. Taking as anchoring point the species currently selected in the NEA-TDB (Ni(cit)$^-$ and $Ni(cit)_2^{4-}$) and based on slope analysis of solubility data (log_{10} [Ni] *vs.* pH_m and log_{10} [Ni] *vs.* log_{10} [cit]), the predominance of the complexes $Ni(H_{-1}cit)^{2-}$, $Ni(OH)(H_{-1}cit)^{3-}$, $Ni(cit)(H_{-1}cit)^{5-}$ and $Ni(H_{-1}cit)_2^{6-}$ at $pH_m \geq 10$ is proposed, with H_{-1}cit corresponding to a citrate ligand with deprotonated alcohol group. The increase in solubility observed in the presence of Ca can only be explained claiming the formation of a quaternary complex, *i.e.*, $Ca[Ni(OH)(H_{-1}cit)]^-$. Based on this chemical model and the fit of solubility data, thermodynamic and SIT activity models were derived for the system Na^+–Ca^{2+}–Ni^{2+}–Cl^-–OH^-–cit^{3-}–H_2O(l). These models can be implemented in thermodynamic databases and geochemical calculations, allowing for the first time an accurate description of Ni(II) solubility and aqueous speciation in citrate-containing cementitious systems.

1. Introduction

The radioactive nickel isotopes ^{59}Ni ($t_{1/2}$–7.6•10^4 a) and ^{63}Ni ($t_{1/2}$–1.0•10^2 a) are activation products of stable isotopes of Ni, Co and Zn present in structural steel and internal components of nuclear reactor vessels. These radionuclides are retained by ion-exchange resins used for the cleaning of the reactor coolant water, which are disposed in repositories for low and intermediate-level waste (L/ILW) (González-Siso et al., 2018; Lindgren et al., 2007).

Cementitious materials are extensively used in repositories for L/ILW for construction purposes and for the stabilization of the waste (Ochs et al., 2016; Wieland, 2014). Upon contact with groundwater, cementitious materials degrade, imposing high alkaline pH conditions (10 ≤ pH ≤ 13.5) in the pore solution over a long-time scale (Duro et al., 2014; Ochs et al., 2016). In CEM I materials (*i.e.*, ordinary Portland cement, OPC), the first degradation stage is characterized by the dissolution of the Na and K hydroxides, resulting in pH values > 13. After the washing out of the alkaline oxides, the second degradation stage proceeds with the dissolution of portlandite ($Ca(OH)_2$), which buffers the porewater composition at pH ≈ 12.5 and [Ca] ≈ 0.02 mol dm^{-3}. The last degradation stage is defined by the incongruent dissolution of calcium silicate hydrate (C–S–H) phases, which evolves from a Ca/Si (C/S) ratio of ≈1.4 (pH ≈ 12.5) to a C/S ≈ 0.6 (pH ≈ 10) (Ochs et al., 2016; Taylor, 1997). These boundary conditions strongly impact the solubility, hydrolysis and complexation properties of the radionuclides present in the waste.

A variety of organic compounds is expected in repositories for L/ILW,

* Corresponding author.
** Corresponding author.
E-mail addresses: oscar.almendros@ciemat.es (O. Almendros-Ginestà), xavier.gaona@kit.edu (X. Gaona).

https://doi.org/10.1016/j.apgeochem.2025.106290
Received 8 October 2024; Received in revised form 17 December 2024; Accepted 21 January 2025
Available online 23 January 2025
0883-2927/© 2025 The Authors. Published by Elsevier Ltd. This is an open access article under the CC BY license (http://creativecommons.org/licenses/by/4.0/).

including decontamination agents (*e.g.*, EDTA, NTA, citrate, *etc.*), cellulose, polymeric materials (plastic, rubber, filter aids, *etc.*), bitumen, as well as cement additives, among others (Duro et al., 2012; Keith-Roach et al., 2021; Keith-Roach and Shahkarami, 2021; Szabo et al., 2023; Tasi et al., 2024; Wieland, 2014). Besides its use in nuclear facilities, citrate is also used as additive in the cement industry to control hardening and other properties of cementitious materials (Guidone et al., 2024; Möschner et al., 2009).

Citrate ($C_6H_8O_7$ as citric acid, see Fig. 1) is a chelating ligand containing four functional groups, *i.e.*, three carboxylates and one hydroxy group. The $pK°_a$ values selected in the NEA-TDB for the first, second, and third carboxylic groups of citric acid are $pK°_{a1} = (3.13 \pm 0.01)$ (H_2cit^-), $pK°_{a2} = (4.78 \pm 0.01)$ ($Hcit^{2-}$) and $pK°_{a3} = (6.36 \pm 0.02)$ (cit^{3-}) (Hummel et al., 2005). The alcohol group of citric acid can deprotonate in very alkaline conditions ($H_{-1}cit^{4-}$, see Hummel et al., 2005 and references therein). No $pK°_{a0}$ is recommended in the NEA-TDB for this species, although a value higher than the $pK°_w$ of water is expected ($pK°_{a0} > 14$). Nevertheless, the coordination of citrate to a metal ion has a strong induction effect, promoting the deprotonation of the alcohol group of the citrate ligand to less alkaline pH values. In the case of Ni(II), the induction effect upon complexation (*e.g.*, formation of $Ni(H_{-1}cit)^{2-}$) is estimated to increase the dissociation constant by more than six orders of magnitude (Hummel et al., 2005).

The formation of strong complexes of citrate with actinides, fission and activation products is described in the literature (Adam et al., 2021; Borkowski et al., 2000; DiBlasi et al., 2023; Felipe-Sotelo et al., 2015; Felmy et al., 2006; Hummel et al., 2005; Keith-Roach and Shahkarami, 2021). Thermodynamic data are available for many of the complexes with citrate forming in acidic conditions, but only a limited number of studies has focused on those complexes forming in alkaline to hyperalkaline pH conditions. In cementitious systems, the impact of citrate (as well as other chelating ligands) in the mobilization of radionuclides is usually considered of minor relevance. This is due to the presence of Ca, which leads to the formation of stable calcium-containing aqueous complexes (*e.g.,* with EDTA, NTA, citrate) and/or solid phases (*e.g.*, with citrate, oxalate) (Hummel et al., 2005; Ochs et al., 2022), that accordingly limit the free ligand concentration available for the complexation with radionuclides.

Thermodynamic data available in the literature for the Ni(II)-cit system were critically reviewed in the 9th volume of the NEA-TDB series (Hummel et al., 2005). Four complexes were selected, *i.e.*, $Ni(H_2cit)^+$, Ni(Hcit)(aq), $Ni(cit)^-$ and $Ni(cit)_2^{4-}$, all of them prevailing in acidic to weakly alkaline pH conditions. The same species are selected in the most relevant thermodynamic databases available in the context of nuclear waste disposal, *e.g.*, PSI-Nagra TDB (Hummel and Thoenen, 2023), ThermoChimie (Giffaut et al., 2014) and JAEA-TDB (Kitamura, 2021).

The formation of Ni(II)-cit complexes involving the deprotonation of the alcohol group of citrate ($H_{-1}cit$), *e.g.*, $Ni(H_{-1}cit)^{2-}$, $Ni(cit)(H_{-1}cit)^{5-}$, $Ni(H_{-1}cit)_2^{6-}$, $Ni_2(cit)(H_{-1}cit)^{3-}$, $Ni_2(H_{-1}cit)_2^{4-}$ and $Ni_4(OH)(H_{-1}cit)_3^{5-}$, has been described in a number of previous publications, mostly involving the use of potentiometric titrations (Daniele et al., 1984, 1988; Heitner-Wirguin et al., 1958; Migal and Sychev, 1958; Patnaik and Pani, 1957, 1965; Salnikov et al., 1984; Sari, 2001). The NEA-TDB disregarded all these studies due to relevant experimental shortcomings. The lack of reliable data for the Ni(II)-cit complexes involving the deprotonation of the alcohol group importantly hinders geochemical calculations for this system in alkaline to hyperalkaline pH conditions.

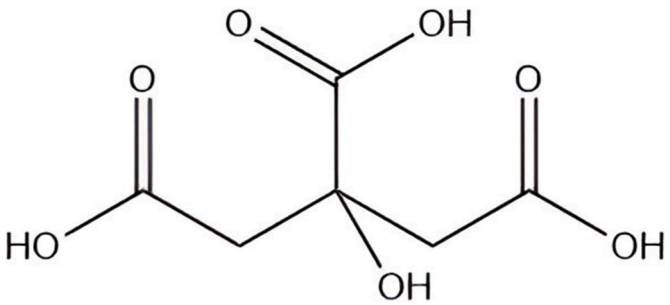

Fig. 1. Molecular structure of citric acid, $C_6H_8O_7$.

In this context, this study aims at investigating the complexation of Ni(II) with citrate in the alkaline to hyperalkaline pH conditions representative of cementitious systems, both in the absence and presence of Ca. For this purpose, systematic undersaturation solubility experiments were conducted at different pH, citrate concentrations and ionic strengths, with the aim of deriving complete chemical, thermodynamic and (SIT) activity models for the system Na^+–Ca^{2+}–Ni^{2+}–Cl^-–OH^-–cit^{3-}–H_2O(l). The use of solubility experiments allows to probe the Ni(II)-citrate system under hyperalkaline conditions, where the low Ni(II) concentrations imposed by the sparingly soluble phase $Ni(OH)_2$(s) prevent the reliable use of potentiometric or spectroscopic methods.

2. Experimental description

2.1. Chemicals

All solutions were prepared with purified water (Milli-Q academic, Millipore), purged for 1.5 h with Ar to remove traces of O_2 and CO_2. All samples were prepared, stored and handled at $T = (22 \pm 2)$ °C inside an inert gas (Ar) glovebox ($O_2 < 5$ ppm) to prevent CO_2 contamination in (hyper)alkaline conditions. NaCl, $Na_3cit(s)\bullet 2H_2O$ and $CaCl_2\bullet 2H_2O$ were obtained from Merck with at least analytical grade purity (≥96%). HCl and NaOH Titrisol © (Merck) were used to adjust the pH of the samples. $Ni(OH)_2$(s) was purchased from Acros Organics, and used as received for the solubility experiments.

2.2. pH measurements

A glass pH electrode (type ROSS, Orion) daily calibrated against dilute standard buffers (pH 4–11, Merck) was used to measure the pH of the investigated samples. Experimentally measured pH values (pH_{exp}) were converted to pH_m (with $pH_m = -\log [H^+]$, and $[H^+]$ in molal units) following the expression $pH_m = pH_{exp} + A_m$, where A_m is an empirical value entailing the activity coefficient of the H^+ and the liquid junction potential of the electrode at the given background electrolyte concentration and temperature. A_m values in NaCl solutions were taken from (Altmaier et al., 2003). In NaCl–NaOH solutions with $[OH^-] > 0.03$ M, the H^+ concentration was calculated from the given $[OH^-]$ and the conditional ion product of water to overcome the alkaline error of the glass electrode. All concentration values quantified in molar units (M) were converted to molality ($mol \cdot kg^{-1}$) using the conversion tables available in the NEA-TDB reference volumes (Grenthe et al., 2020).

2.3. Solubility experiments with $Ni(OH)_2$(s) and citrate in the absence and presence of ca

Batch solubility experiments were conducted from undersaturation conditions using a commercial, well-characterized $Ni(OH)_2$(s). A few milligrams (5–10) of the original material were transferred to a capped silicon single crystal sample holder (Dome, Bruker). X-ray diffraction patterns were collected with a Bruker AXS D8 Advance X-ray powder diffractometer at angles $2\theta = 8$–$80°$, with incremental steps of 0.01° and accumulation time of 1 s per step.

A total of 79 independent batch samples were prepared using *ca.* 20 mg of β-$Ni(OH)_2$(cr) in 25 mL solution per experiment. Seven series of solubility experiments were conducted at constant ionic strength in 0.1, 0.5, 1.0 and 3.0 mol dm^{-3} NaCl–NiOH–Na_3Cit solutions with $5 \cdot 10^{-5}$ mol $dm^{-3} \leq [cit]_{tot} \leq 0.1$ mol dm^{-3} and $9.0 \leq pH_m \leq 13.5$. To evaluate the possible impact of Ca on the complexation of Ni(II) with citrate,

three additional series with 12 independent batch samples were prepared in 0.1, 1.0 and 3.0 mol dm^{-3} NaCl–NiOH–Na_3Cit solutions containing 0.02 mol dm^{-3} $CaCl_2$. The pH_m of the latter samples was limited to 12.4 to minimize the precipitation of portlandite, whereas citrate concentration in these series was restricted to 10^{-3} mol dm^{-3} to avoid the precipitation of $Ca_3Cit_2{\cdot}4H_2O$(cr) (Hummel et al., 2005). The saturation index of $Ca_3Cit_2{\cdot}4H_2O$(cr) was <0 in all investigated systems. Experimental conditions in all solubility experiments are summarized in Table 1.

The pH_m and [Ni] were monitored for up to 360 days. The concentration of Ni was determined by inductively coupled plasma mass spectrometry (ICP-MS, iCAP TQs Thermo Scientific™ equipment) after phase separation by ultrafiltration with 10 kD filters (2–3 nm cut-off, Nanosep® centrifuge tubes, Pall Life Sciences).

3. Results and discussion

3.1. Solid phase characterization

Fig. 2 shows the XRD characterization of the original $Ni(OH)_2$(s) material as well as selected Ni(II) solid phases after completing the solubility experiments, *i.e.*, equilibrated in 0.1, 1.0 mol dm^{-3} and 3.0 mol dm^{-3} NaCl solutions containing citrate, both in the absence and in the presence of 0.02 mol dm^{-3} Ca. The comparison of the diffraction patterns with of the original material with reference data confirmed the only presence of crystalline β-$Ni(OH)_2$(cr) (PDF 73–1520, see also (Palmer and Gamsjäger, 2010)). For the solids collected after terminating the solubility experiments, a perfect match is obtained also in all cases with the reference diffractogram of β-$Ni(OH)_2$(cr) (PDF 73–1520), thus confirming that the solubility of Ni(II) in the investigated systems is controlled by this solid phase. Additional patterns observed in the solid phases equilibrated in 3.0 mol dm^{-3} NaCl perfectly match reference data available for NaCl (PDF 05–0628). This indicates that the washing steps (3 times with ethanol) were insufficient to completely remove the background electrolyte. The absence of any additional feature in the diffractograms of the systems containing both Ca and citrate underpins that $Ca_3Cit_2{\cdot}4H_2O$(cr) did not precipitate in the course of the solubility experiments. This is in line with thermodynamic calculations, which predicted a negative saturation index for this solid phase within the boundary conditions considered in this study.

3.2. Solubility of Ni(II) in NaCl–NaOH–Na_3cit systems in the absence of ca

The solubility of Ni(II) determined in NaCl–NaOH–Na_3cit systems with $9.5 \le pH_m \le 13.5$ and $5{\cdot}10^{-5}$ mol $kg^{-1} \le [cit]_{tot} \le 0.1$ mol kg^{-1} are shown in Fig. 3 ($I = 0.1$ and 0.5 mol dm^{-3}) and Fig. 4 ($I = 1.0$ and 3.0 mol dm^{-3}). Symbols in the figures correspond to individual measurements of the batch samples summarized in Table 1. Dispersion of the data reflect the uncertainties in pH and [Ni(II)] measurements, and generally does not correspond to trends in solubility. However, slow dissolution kinetics were observed in solubility samples at $pH_m < 9.5$ (see Figs. SI–1 in the Supporting Information), which prevented the attainment of equilibrium conditions in this pH_m-region. These samples were not included in the thermodynamic evaluation in this study.

Black solid lines in the figures correspond to the solubility of β-$Ni(OH)_2$(cr) calculated for the corresponding ionic strength conditions using thermodynamic data reported in (González-Siso et al., 2018), whereas dotted lines in the figures indicate the solubility of β-$Ni(OH)_2$(cr) in the presence of citrate, calculated considering the given experimental conditions and the current NEA-TDB thermodynamic selection for the system Ni(II)-cit.

Figs. 3 and 4 show that the Ni(II) solubility in presence of citrate is clearly above citrate-free systems in most of the investigated conditions and for the complete pH_m range evaluated. In 0.1 M NaCl systems with $[cit]_{tot} = 1{\cdot}10^{-4}$ and $1{\cdot}10^{-3}$ mol kg^{-1} (Fig. 3a), experimental solubility data are satisfactorily explained by thermodynamic calculations using the NEA-TDB selection. At these ionic strength and citrate concentrations, Ni(II)-cit complexes dominate the aqueous speciation of Ni(II) only at pH_m below ≈ 11.3 (precise pH depending upon ligand concentration), whereas they are outcompeted by hydrolysis (*i.e.*, predominance of $Ni(OH)_2$(aq)) above this pH_m.

Fig. 3b shows the solubility of Ni(II) in $I = 0.1$ mol dm^{-3} solutions at $pH_m = 10$ and varying citrate concentrations. Experimental data displayed in the figure are correctly explained by the solubility calculations using the current NEA-TDB thermodynamic selection, which predicts the predominance of the complex $Ni(cit)^-$ over almost the complete range of citrate concentrations investigated. Fig. 3c summarizes the experimental solubility data of Ni(II) determined in the presence of citrate at $I = 0.5$ mol dm^{-3}. At $pH_m \le 11$, experimental data are properly explained by model calculations using the NEA-TDB selection. However, as reflected by the mismatch between the experimental data and thermodynamic calculations at higher pH_m values, the solubility cannot be explained alone by aqueous complexes currently selected in NEA-TDB, *i.e.*, $Ni(cit)^-$ and $Ni(cit)_2^{4-}$. This suggests that additional Ni(II)–cit complexes expectedly involving Ni(II) hydrolysis, deprotonation of the alcohol group of citrate, or both, seem to be required in order to complete the chemical model of the Ni(II)–cit–H_2O(l) system. The mismatch between experimental solubility data and model calculations becomes more evident in Fig. 4, which shows solubility data collected at $I = 1.0$ and 3.0 mol dm^{-3} at higher ligand concentrations. A moderate to good agreement between experimental and calculated solubility is only observed in Fig. 4b (log [Ni(II)] *vs.* $[cit]_{tot}$ at $pH_m = 11.2$), which possibly reflects the predominance of the complexes $Ni(cit)^-$ and $Ni(cit)_2^{4-}$ at these pH_m and ionic strength conditions.

Fig. 3b, 4b and 4d (log [Ni(II)] *vs.* log $[cit]_{tot}$) support that much stronger complexation takes place at $pH_m \le 10$, where the unhydrolyzed Ni^{2+} species prevails in the absence of citrate. Complexation becomes weaker with increasing pH_m due to the expected competition with hydrolysis. However, complexation takes place at $[cit]_{tot} \ge 10^{-3}$ mol kg^{-1} at $pH_m \approx 11$ and at $[cit]_{tot} \ge 10^{-2}$ mol kg^{-1} at $pH_m \approx 13$, thus evidencing that citrate can outcompete hydrolysis in hyperalkaline pH_m conditions at intermediate to high ligand concentrations.

The use of a background electrolyte of sufficiently high

Table 1
Experimental conditions in the investigated solubility samples.

Series	I (mol·dm^{-3})	pH_m	[cit] (mol·dm^{-3})	[Ca] (mol·dm^{-3})	n° samples
Absence of Ca *(pH-variation)*	0.1	9.0–13.0	$1{\bullet}10^{-4}$ – $1{\cdot}10^{-3}$	–	14
	0.5	9.0–13.5	$1{\cdot}10^{-2}$	–	10
	1.0	9.0–13.5	$8{\cdot}10^{-3}$–$5{\cdot}10^{-2}$	–	16
	3.0	9.0–13.5	$5{\cdot}10^{-3}$–$5{\cdot}10^{-2}$	–	16
Absence of Ca *([Cit]-variation)*	0.1	10.0	$5{\bullet}10^{-5}$ – $5{\bullet}10^{-3}$	–	5
	1.0	11.2	$5{\bullet}10^{-3}$ – 0.1	–	5
	3.0	13.0	$5{\bullet}10^{-3}$ – 0.1	–	6
Presence of Ca *(pH-variation)*	0.1, 1.0, 3.0	9.0–12.4	$1{\bullet}10^{-3}$	0.02	12

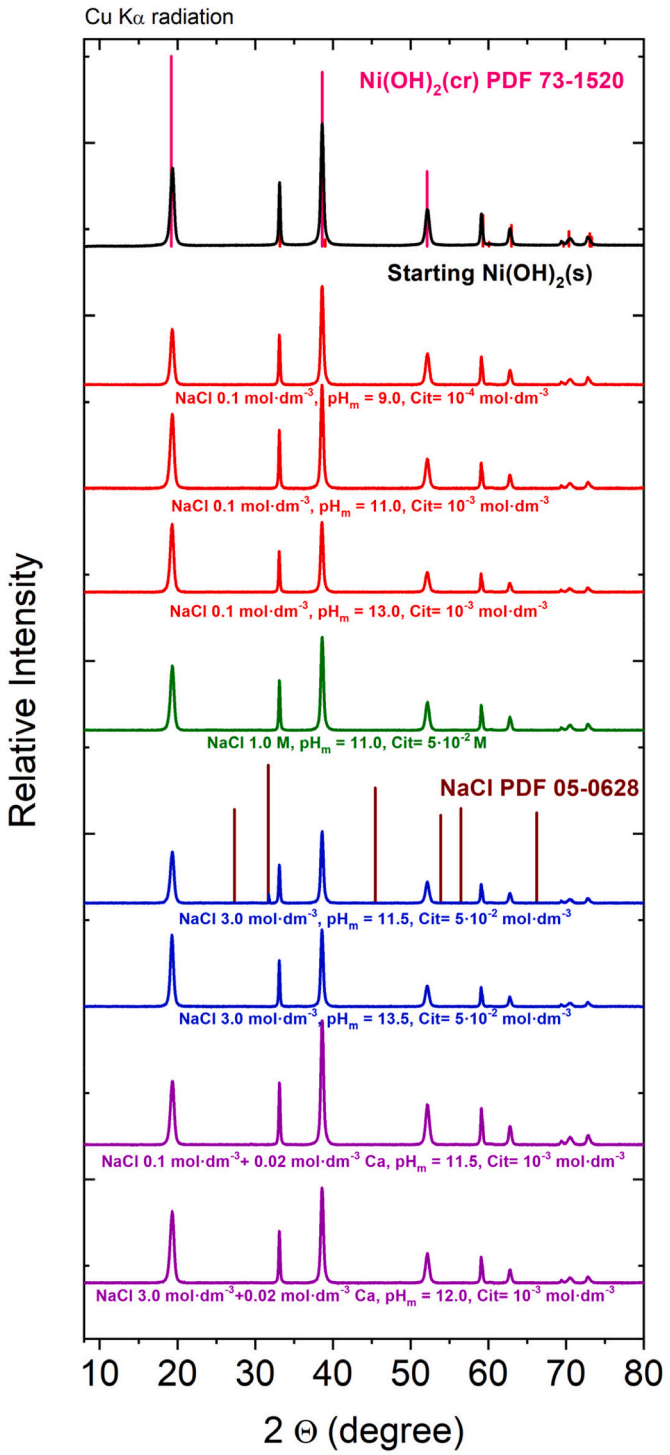

Fig. 2. Diffractograms of Ni(II) solid phases collected from selected solubility experiments in 0.1, 1.0 and 3.0 mol dm^{-3} NaCl–CaCl2–NaOH–Na3cit. The diffractogram of the original Ni(OH)2(s) material is included for comparison. Dark pink and brown lines correspond to reference patterns for β-$Ni(OH)_2$(cr) (PDF 73–1520) and NaCl (PDF 05–0628), respectively.

concentration allows ensuring constant activity factors in the equilibrium experiments. On this basis, slope analysis of the solubility data gives insight on the stoichiometries Ni:OH (log [Ni(II)] *vs.* pH_m) and Ni:cit (log [Ni(II)] *vs.* $[cit]_{free}$). Note that for Ca-free systems, the relationship $[cit]_{free} \approx [cit]_{tot}$ can be safely assumed. Three main regimes can be identified in the experiments at constant ligand concentration and varying pH_m: (i) slope of −2 in the less alkaline pH_m-region, indicating that two protons are released in the equilibrium reaction controlling the solubility. Considering a solubility-control by β-Ni$(OH)_2$(cr) as confirmed in Section 3.1, the aqueous speciation in this pH_m-region is expectedly dominated by the complexes already selected in the NEA-TDB, *i.e.*, $Ni(cit)^-$ and $Ni(cit)_2^{4-}$; (ii) slope of −1 within $pH_m \approx 10.5$ and ≈12 (precise pH_m-range depending upon ionic strength), corresponding to the release of one H^+ in the equilibrium reaction controlling solubility; (iii) slope of 0 within $pH_m \approx 12$ and ≈13.5 (precise pH_m-range depending upon ionic strength), which underpins the predominance of a solubility reaction involving no exchange of protons. In the absence of citrate, the pH_m-independent reaction controlling the solubility of Ni(II) at $10 \leq pH_m \leq 13.5$ is defined as β-$Ni(OH)_2$(cr) ⇔ Ni$(OH)_2$(aq). In the presence of citrate, such behaviour can be explained by the predominance of $Ni(OH)_2(cit)^{3-}$ (alternatively $Ni(OH)(H_{-1}cit)^{3-}$) and/or $Ni(OH)_2(cit)_2^{6-}$ (alternatively $Ni(H_{-1}cit)_2^{6-}$). Note that strong interactions of such highly charged species are to be expected with other cations present in solution (see also discussion in Section 3.4).

Felipe-Sotelo and co-workers conducted oversaturation solubility experiments with different radionuclides (Ni(II), Th(IV), U(IV) and U(VI)) in the presence of organic ligands (citrate, EDTA and DTPA) (Felipe-Sotelo et al., 2015). Experiments were performed at pH ≈ 12.3 with $5\bullet10^{-3}$ mol $dm^{-3} \leq [cit]_{tot} \leq 0.1$ mol dm^{-3}, in the absence and presence of calcium ($5\bullet10^{-3}$ mol $dm^{-3} \leq [Ca] \leq 2\bullet10^{-2}$ mol dm^{-3}). In the presence of $[cit]_{tot} = 0.01$ mol dm^{-3} and absence of Ca, the authors reported a solubility of nickel in the range of 10^{-5}–10^{-4} mol dm^{-3}, *i.e.*, approximately 2 orders of magnitude greater than the corresponding citrate-free systems. They concluded that such an increase could not be explained with the current NEA-TDB thermodynamic selection. The overall solubilities reported by Felipe-Sotelo and co-workers are clearly higher than those determined in this work (Figs. 1 and 5 in Felipe-Sotelo et al., 2015), but the trends and conclusions are similar. Note that the enhanced Ni(II) concentrations compared to the current study is possibly due to the formation of a less crystalline solid phase when approaching the system from oversaturation conditions.

Patnaik and Pani investigated the solubility of $Ni(OH)_2$(s) in the presence of citrate at $T = 35$ °C and weakly alkaline conditions ($7.5 \leq pH \leq 9.5$) (Patnaik and Pani, 1965). Solubility experiments were complemented with pH titrations and conductimetric methods. Based on their observations, the authors proposed the formation of 1:1 complexes with charge −1 and −2, which can be matched with $Ni(cit)^-$ and $Ni(H_{-1}cit)^{2-}$. Note that the NEA-TDB disregarded any data selection from this reference due to relevant experimental shortcomings (Hummel et al., 2005).

3.3. Solubility of Ni(II) in NaCl–NaOH–Na_3cit systems in the presence of ca

Fig. 5 shows the experimental solubility data determined in NaCl–NaOH–Na_3cit systems containing $[cit]_{tot} = 1\bullet10^{-3}$ mol kg^{-1} and [Ca] = 0.02 mol kg^{-1}. The figure shows also the solubility of β-Ni$(OH)_2$(cr) calculated for the same boundary conditions using the Ni(II) solubility and hydrolysis constants reported in (González-Siso et al., 2018) and the Ni(II)-cit complexation constants currently selected in the NEA-TDB (Hummel et al., 2005).

Solubility data determined in the pH_m-region 9–10 shows a slight increase in [Ni] compared to the citrate-free system (black line in the figure). This increase is well-reproduced by thermodynamic calculations, which predict the predominance of the binary complex $Ni(cit)^-$ in this pH_m-region. Solubility data above $pH_m \approx 11$ shows a pH_m-independent behaviour for the three investigated ionic strength conditions, *i.e.*, 0.1, 1.0 and 3.0 mol dm^{-3} NaCl–NaOH–Na_3cit. Experimentally measured Ni(II) concentrations are again higher than those expected for citrate-free systems. However, thermodynamic calculations do not predict any solubility enhancement due to the predominance of the hydrolysis species $Ni(OH)_2$(aq) and the competition with Ca^{2+} for the complexation with citrate. The disagreement between experimental

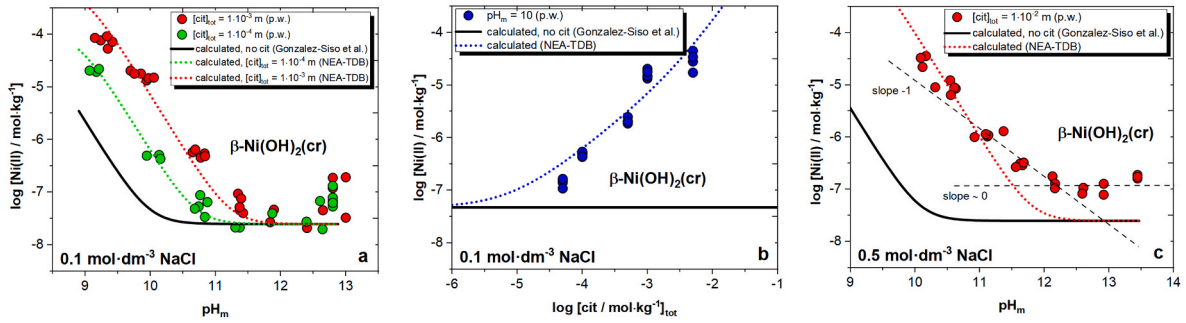

Fig. 3. Solubility of Ni(II) determined in NaCl–NaOH–Na_3cit systems with (a) I = 0.1 mol dm^{-3}, $[cit]_{tot} = 1{\cdot}10^{-4}$, $1{\cdot}10^{-3}$ mol kg^{-1} and $9.5 \leq pH_m \leq 12.8$; (b) I = 0.1 mol dm^{-3}, $pH_m = 10.0$ and $5{\cdot}10^{-5}$ mol $kg^{-1} \leq [cit]_{tot} \leq 5{\cdot}10^{-3}$ mol kg^{-1}; and (c) I = 0.5 mol dm^{-3}, $[cit]_{tot} = 1{\cdot}10^{-2}$ mol kg^{-1} and $10 \leq pH_m \leq 13.5$. Black solid and colored dotted lines correspond to the solubility of β-$Ni(OH)_2$(cr) calculated in the absence and presence of citrate, respectively. Calculations performed using thermodynamic data reported by González-Siso et al. (solubility and hydrolysis) and selected in the NEA-TDB (Ni(II)-cit system).

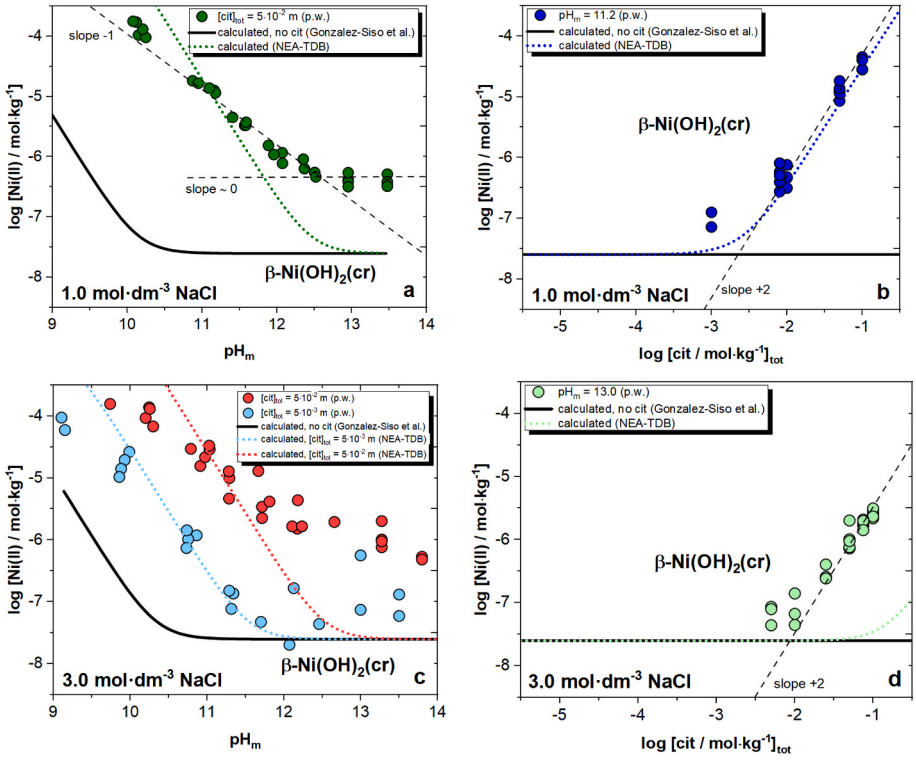

Fig. 4. Solubility of Ni(II) determined in NaCl–NaOH–Na_3cit systems with (a) I = 1.0 mol dm^{-3}, $[cit]_{tot} = 5{\cdot}10^{-2}$ mol kg^{-1} and $10 \leq pH_m \leq 13.5$; (b) I = 1.0 mol dm^{-3}, $pH_m = 11.2$ and $1{\cdot}10^{-3}$ mol $kg^{-1} \leq [cit]_{tot} \leq 0.1$ mol kg^{-1}; (c) I = 3.0 mol dm^{-3}, $[cit]_{tot} = 5{\cdot}10^{-3}$, $5{\cdot}10^{-2}$ mol kg^{-1} and $10 \leq pH_m \leq 13.5$; and (d) I = 3.0 mol dm^{-3}, $pH_m = 13.0$ and $5{\cdot}10^{-3}$ mol $kg^{-1} \leq [cit]_{tot} \leq 0.1$ mol kg^{-1}. Black solid and colored dotted lines correspond to the solubility of β-$Ni(OH)_2$(cr) calculated in the absence and presence of citrate, respectively. Calculations performed using thermodynamic data reported by González-Siso et al. (solubility and hydrolysis) and selected in the NEA-TDB (Ni(II)–cit system).

solubility and model calculations provide indirect evidence on the formation of quaternary complexes of the type Ca–Ni(II)–OH-cit. A similar hypothesis was raised by Felipe-Sotelo and co-workers on the basis of their solubility experiments with the Ni(II)-cit system at $pH_m \approx 12.3$, conducted in the absence and presence of Ca (Felipe-Sotelo et al., 2015).

3.4. *Chemical, thermodynamic and SIT activity models for the system* Na^+–Ca^{2+}–Ni^{2+}–Cl^-–OH^-–cit^{3-}–H_2O(l)

Thermodynamic data in the reference state describing the Na^+–Ca^{2+}–Ni^{2+}–Cl^-–OH^-–cit^{3-}–H_2O(l) systems were determined on the basis of solubility data obtained in this work at $I = 0.1$, 0.5, 1.0 and 3.0 mol dm^{-3} in NaOH–NaCl–$CaCl_2$–Na_3cit solutions, in combination with solid phase characterization by XRD. The binary complexes $Ni(cit)^-$ and $Ni(cit)_2^{4-}$, prevailing in weakly acidic to weakly alkaline conditions and currently selected in the NEA–TDB, have been taken as anchoring point to extend the chemical model in the alkaline to hyperalkaline pH region. Differences between thermodynamic constants at $T = 22$ °C and in the reference state ($T = 25$ °C) are significantly lower than the experimental uncertainty in solubility data. No temperature corrections have been accordingly performed.

The specific ion interaction theory (SIT) has been considered to account for ionic strength corrections (Ciavatta, 1980), in agreement with the approach favored within the NEA-TDB project (Grenthe et al., 2020; Hummel et al., 2005). In SIT, activity coefficients γ_j are calculated as described in equation (1):

$$\log_{10} \gamma_j = -z_j^2 D + \sum \varepsilon(j, k, I_m)\, m_k \quad (1)$$

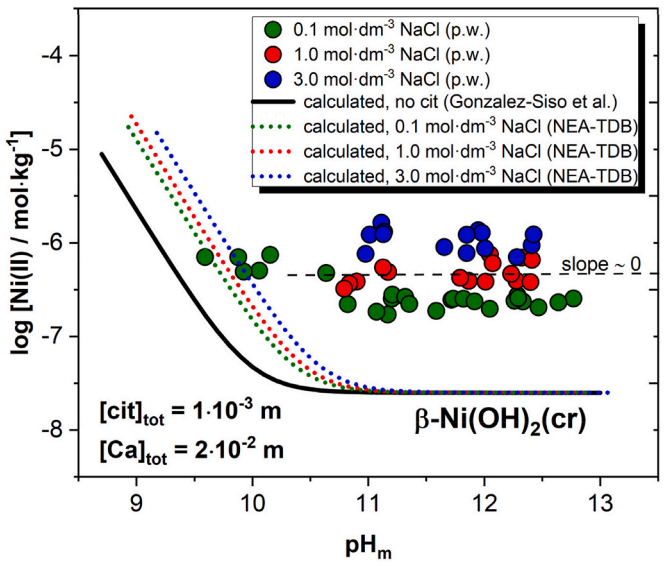

Fig. 5. Solubility of Ni(II) determined in NaCl–NaOH–Na_3cit systems with $[cit]_{tot} = 1 \bullet 10^{-3}$ mol kg^{-1}, [Ca] = 0.02 mol kg^{-1}, at I = 0.1 mol dm^{-3} (green symbols), 1.0 mol dm^{-3} (blue symbols) and 3.0 mol dm^{-3} (red symbols). Black solid and colored dotted lines correspond to the solubility of β-$Ni(OH)_2$(cr) calculated in the absence and presence of citrate, respectively. Calculations performed using thermodynamic data reported by González-Siso et al. (solubility and hydrolysis) and selected in the NEA-TDB (Ni(II)–cit system).

where D is the Debye-Hückel term, z_j the charge of an ion j, I_m the molal ionic strength, m_k the molality of all ions k present in the solution and $\varepsilon(j, k, I_m)$ the specific ion interaction parameter.

As discussed in Section 3.2, the binary complexes $Ni(cit)^-$ and $Ni(cit)_2^{4-}$ currently selected in the NEA-TDB can only explain experimental solubility data determined in this work under moderately alkaline pH conditions ($pH_m \leq 10.5$). At higher pH_m values, and particularly at $I \geq 0.5$ mol dm^{-3} NaCl–NaOH–Na_3cit, discrepancies between model calculations and experimental data become very evident, supporting the formation of additional Ni(II)-cit complexes. Slope analysis (log [Ni(II)] *vs.* pH_m and log [Ni(II)] *vs.* log $[cit]_{tot}$) in these pH_m-regions underpin the predominance of the limiting complexes $Ni(cit)(H_{-1}cit)^{5-}$ and $Ni(H_{-1}cit)_2^{6-}$, according with the equilibrium reactions (2) and (3). It is to be expected that such negatively charged complexes interact strongly with Na^+ cations in the background electrolyte, and thus form complexes of the type $Na_xNi(cit)(H_{-1}cit)^{(5-x)-}$ and $Na_yNi(H_{-1}cit)_2^{(6-y)-}$ in the conditions of this study. Because of the challenging determination of the ratio Na:Ni, and particularly to avoid an overparameterization in the thermodynamic model, the formation of ternary complexes Na–Ni(II)-cit has been excluded from the chemical model. Although acknowledging that these interactions can be very relevant, they are accounted for in the activity model through the SIT coefficients.

$$\beta\text{-}Ni(OH)_2(cr) + 2cit^{3-} + H^+ \Leftrightarrow Ni(cit)(H_{-1}cit)^{5-} + 2H_2O(l) \quad (2)$$

(slope −1: log [Ni(II)] vs. pH_m//slope +2: log [Ni(II)] *vs.* log $[cit]_{tot}$)

$$\beta\text{-}Ni(OH)_2(cr) + 2cit^{3-} \Leftrightarrow Ni(H_{-1}cit)_2^{6-} + 2H_2O(l) \quad (3)$$

(slope 0: log [Ni(II)] vs. pH_m//slope +2: log [Ni(II)] *vs.* log $[cit]_{tot}$)

with the conditional solubility constants at given ionic strength:

$$\log {}^*K'_{s,(1,0,2,-1)} = \log [Ni(cit)(H_{-1}cit)^{5-}] + pH_m - 2 \log [cit^{3-}] \quad (4)$$

$$\log {}^*K'_{s,(1,0,2,-2)} = \log [Ni(H_{-1}cit)_2^{6-}] - 2 \log [cit^{3-}] \quad (5)$$

with p, x, y, z in $\log {}^*K'_{s,(p,x,y,z)}$ corresponding to the stoichiometric numbers in the complex: p = Ni, x = Ca, y = cit and z = number of H^+ involved in the complexation reaction (either as hydrolysis of water or deprotonation of alcohol group of citrate). Solubility constants at the reference state can be accordingly calculated.$\log {}^*K^\circ_{s,(1,0,2,-1)} = \log {}^*K'_{s,(1,0,2,-1)} - \log \gamma(Ni(cit)(H_{-1}cit)^{5-})$

$$+ \log \gamma(H^+) + 2 \log \gamma(cit^{3-}) - 2 \log a_w \quad (6)$$

$$\log {}^*K^\circ_{s,(1,0,2,-2)} = \log {}^*K'_{s,(1,0,2,-2)} - \log \gamma(Ni(H_{-1}cit)_2^{6-}) + 2 \log \gamma(cit^{3-}) - 2 \log a_w \quad (7)$$

At high ligand concentrations, the formation of these complexes defines a consistent trend building as anchoring point on the current NEA-TDB selection, *i.e.*, $Ni(cit)_2^{4-} \rightarrow Ni(cit)(H_{-1}cit)^{5-} \rightarrow Ni(H_{-1}cit)_2^{6-}$. A first attempt to model the solubility data in Ca-free systems using this chemical model was not satisfactory due to discrepancies with experimental data at low ligand concentrations. For this reason, the 1:1 complexes $Ni(H_{-1}cit)^{2-}$ and $Ni(OH)(H_{-1}cit)^{3-}$ were also included in the chemical model according with reactions (8) and (9):

$$\beta\text{-}Ni(OH)_2(cr) + Cit^{3-} + H^+ \Leftrightarrow Ni(H_{-1}cit)^{2-} + 2H_2O(l) \quad (8)$$

(slope −1: log [Ni(II)] vs. pH_m//slope +1: log [Ni(II)] *vs.* log $[cit]_{tot}$)

$$\beta\text{-}Ni(OH)_2(cr) + cit^{3-} \Leftrightarrow Ni(OH)(H_{-1}cit)^{3-} + H_2O(l) \quad (9)$$

(slope 0: log [Ni(II)] vs. pH_m//slope +1: log [Ni(II)] *vs.* log $[cit]_{tot}$)

with the conditional solubility constants at given ionic strength:

$$\log {}^*K'_{s,(1,0,1,-1)} = \log [Ni(H_{-1}cit)^{2-}] + pH_m - \log [cit^{3-}] \quad (10)$$

$$\log {}^*K'_{s,(1,0,1,-2)} = \log [Ni(OH)(H_{-1}cit)^{3-}] - \log [cit^{3-}] \quad (11)$$

and the corresponding solubility constants at the reference state:

$\log {}^*K^\circ_{s,(1,0,1,-1)} = \log {}^*K'_{s,(1,0,1,-1)} - \log \gamma(Ni(H_{-1}cit)^{2-})$

$$+ \log \gamma(H^+) + \log \gamma(cit^{3-}) - 2 \log a_w \quad (12)$$

$$\log {}^*K^\circ_{s,(1,0,1,-2)} = \log {}^*K'_{s,(1,0,1,-2)} - \log \gamma(Ni(OH)(H_{-1}cit)^{3-}) + \log \gamma(cit^{3-}) - \log a_w \quad (13)$$

In spite of the large pool of data collected in Ca-free systems (9 independent series, ≈150 independent solubility measurements), the complexity of the system and the number of variables to be fitted ($\log {}^*K^\circ_{s,(1,0,1,-1)}$, $\log {}^*K^\circ_{s,(1,0,1,-2)}$, $\log {}^*K^\circ_{s,(1,0,2,-1)}$, $\log {}^*K^\circ_{s,(1,0,2,-2)}$, $\varepsilon(Ni(H_{-1}cit)^{2-}, Na^+)$, $\varepsilon(Ni(OH)(H_{-1}cit)^{3-}, Na^+)$, $\varepsilon(Ni(cit)_2^{4-}, Na^+)$, $\varepsilon(Ni(cit)(H_{-1}cit)^{5-}, Na^+)$, $\varepsilon(Ni(H_{-1}cit)_2^{6-}, Na^+)$) for the development of a complete model required the use of a step-wise approach. In a first step, tentative SIT-plots were prepared for limiting complexes, in order to gain a first insight on the values of $\log {}^*K^\circ_{s,(1,x,y,z)}$ and SIT coefficients of these complexes (see Figs. SI–2 in the Supporting Information). In a second step, all parameters were taken into account and the difference between experimental and calculated Ni(II) concentrations minimized. In this process, it became evident that the value of $\log {}^*K^\circ_{s,(1,0,2,0)}$ (*i.e.*, corresponding to $Ni(cit)_2^{4-}$) currently selected in the NEA-TDB systematically led to an overestimation of the experimental solubility data in the less alkaline pH_m-region, and thus was also included in the optimization process. Solubility constants $\log {}^*K^\circ_{s,(1,x,y,z)}$ and SIT coefficients resulting from this fit are summarized in Tables 2 and 3, respectively. Table 2 includes also the equilibrium constants $\log {}^*\beta^\circ_{(1,x,y,z)}$, calculated combining the solubility constants $\log {}^*K^\circ_{s,(1,x,y,z)}$ and the solubility product $\log {}^*K^\circ_{s,0}$ reported for β-$Ni(OH)_2$(cr) in (González-Siso et al., 2018).

The equilibrium constant derived in this work for the formation of the complex $Ni(cit)_2^{4-}$ is clearly lower than the current selection in the NEA-TDB, although both values agree within their corresponding uncertainties ($\log {}^*\beta^\circ_{(1,0,2,0)} = (7.7 \pm 0.4)$ (this work) *vs.* $\log {}^*\beta^\circ_{(1,0,2,0)} = (8.5 \pm 0.4)$ (Hummel et al., 2005)). We note that the NEA-TDB selection is based on a single potentiometric study conducted in 0.1 M KCl (Hedwig et al., 1980). The value of $\log {}^*\beta^\circ_{(1,0,2,0)}$ selected by the NEA-TDB reviewers was obtained by neglecting the $\Delta\varepsilon \cdot I_m$ term at $I = 0.1$ M KCl, and assigning a larger uncertainty.

The pH_m-independent solubility behaviour in the Ca-containing systems (see Fig. 4) indicates that no H^+ are involved in the

Table 2
Summary of the solubility and complexation constants for the Na^+–Ca^{2+}–Ni^{2+}–Cl^-–OH^-–cit–H_2O(l) system, as determined in this work or reported in the literature. Values reported in the reference state (T = 25 °C and I = 0).

Chemical reaction	Equilibrium constant	Reference
β-$Ni(OH)_2$(cr) + $2H^+$ ⇄ Ni^{2+} + $2H_2O$(l)	(12.10 ± 0.11)	(González-Siso et al., 2018)
β-$Ni(OH)_2$(cr) + cit^{3-} + $2H^+$ ⇄ Ni(cit)$^-$ + $2H_2O$(l)	(18.86 ± 0.14)	(Hummel et al., 2005) ([a])
β-$Ni(OH)_2$(cr) + cit^{3-} + H^+ ⇄ $Ni(H_1cit)^{2-}$ + $2H_2O$(l)	(7.8 ± 0.3)	This work
β-$Ni(OH)_2$(cr) + cit^{3-} ⇄ $Ni(OH)(H_1cit)^{3-}$ + H_2O(l)	–(5.1 ± 0.4)	This work
β-$Ni(OH)_2$(cr) + $2cit^{3-}$ + $2H^+$ ⇄ $Ni(cit)_2^{4-}$ + $2H_2O$(l)	(19.8 ± 0.4) (20.6 ± 0.4)	This work (Hummel et al., 2005) ([a])
β-$Ni(OH)_2$(cr) + $2cit^{3-}$ + H^+ ⇄ $Ni(cit)(H_1cit)^{5-}$ + $2H_2O$(l)	(7.4 ± 0.3)	This work
β-$Ni(OH)_2$(cr) + $2cit^{3-}$ ⇄ $Ni(H_1cit)_2^{5-}$ + $2H_2O$(l)	–(7.9 ± 0.4)	This work
β-$Ni(OH)_2$(cr) + Ca(cit)$^-$ ⇄ $Ca[Ni(OH)(H_1cit)]^-$ + H_2O(l)	–(3.6 ± 0.3)	This work
$Ca_3(cit)_2{\cdot}4H_2O$(cr) ⇄ $3Ca^{2+}$ + $2cit^{3-}$ + $4H_2O$(l)	–(17.9 ± 0.1)	Hummel et al. (2005)
$Ca(OH)_2$(cr) + $2H^+$ ⇄ Ca^{2+} + $2H_2O$(l)	(22.81 ± 0.05)	Giffaut et al. (2014)
Ni^{2+} + $2H_2O$(l) ⇄ $Ni(OH)_2$(aq) + $2H^+$	–(19.7 ± 0.4)	(González-Siso et al., 2018)
Ni^{2+} + Cl^- ⇄ $NiCl^+$	(0.08 ± 0.60)	Gamsjäger et al. (2005)
Ni^{2+} + cit^{3-} ⇄ Ni(cit)$^-$	(6.76 ± 0.08)	Hummel et al. (2005)
Ni^{2+} + cit^{3-} ⇄ $Ni(H_1cit)^{2-}$ + H^+	–(4.3 ± 0.3)	This work ([b])
Ni^{2+} + H_2O(l) + cit^{3-} ⇄ $Ni(OH)(H_1cit)^{3-}$ + $2H^+$	–(17.2 ± 0.4)	This work ([b])
Ni^{2+} + $2cit^{3-}$ ⇄ $Ni(cit)_2^{4-}$	(7.7 ± 0.4) (8.5 ± 0.4)	This work ([b]) Hummel et al. (2005)
Ni^{2+} + $2cit^{3-}$ ⇄ $Ni(cit)(H_1cit)^{5-}$ + H^+	–(4.7 ± 0.3)	This work ([b])
Ni^{2+} + $2cit^{3-}$ ⇄ $Ni(H_1cit)_2^{6-}$ + $2H^+$	–(20.0 ± 0.4)	This work ([b])
Ni^{2+} + Ca^{2+} + cit^{3-} + H_2O(l) ⇄ $Ca[Ni(OH)(H_1cit)]^-$ + $2H^+$	–(10.9 ± 0.3)	This work ([c])
Ca^{2+} + cit^{3-} ⇄ Ca(cit)$^-$	(4.8 ± 0.03)	Hummel et al. (2005)

[a] Solubility constant calculated combining the complexation constant selected in (Hummel et al., 2005) and the solubility product of β-$Ni(OH)_2$(cr) reported in (González-Siso et al., 2018).
[b] Complexation constant calculated combining the solubility constant determined in this work and the solubility product of β-$Ni(OH)_2$(cr) reported in (González-Siso et al., 2018).
[c] Complexation constant calculated combining the solubility constant determined in this work, the solubility product of β-$Ni(OH)_2$(cr) reported in (González-Siso et al., 2018) and the equilibrium constant selected in (Hummel et al., 2005) for the complex Ca(cit)$^-$.

equilibrium reaction controlling the solubility under the investigated conditions. At [cit] = $1{\bullet}10^{-3}$ mol kg^{-1}, solubility experiments in Ca-free systems support the predominance of complexes with a Ni:cit ratio of 1:1, and the same stoichiometry has been considered for the ternary complex with Ca. The solubility reaction (14) is thus defined for Ca-containing systems, under the assumption that the number of Ca atoms participating in the complex formation is also one. Model calculations including two Ca atoms did not improve the quality of the fit.

In order to describe the chemical equilibrium under the more realistic conditions, the solubility reaction was defined in terms of the predominant components in the system, *i.e.*, β-$Ni(OH)_2$(cr) and Ca(cit)$^-$.

$$\beta\text{-}Ni(OH)_2(cr) + Ca(cit)^- \Leftrightarrow Ca[Ni(OH)(H_1cit)]^- + H_2O(l) \quad (14)$$

with the conditional solubility constant at a given ionic strength:

$$\log {}^*K'_{s,(1,1,1,-1)} = \log [Ca[Ni(OH)(H_1cit)]^-] - \log [Ca(cit)^-] \quad (15)$$

and the corresponding solubility constant at the reference state:

$$\log {}^*K^\circ_{s,(1,1,1,-1)} = \log {}^*K'_{s,(1,1,1,-1)} - \log \gamma(Ca[Ni(OH)(H_1cit)]^-) + \log \gamma(Ca(cit)^-) - \log a_w \quad (16)$$

The resulting solubility and equilibrium constants (log ${}^*K^\circ_{s,(1,1,1,-1)}$ and log ${}^*\beta^\circ_{(1,1,1,-1)}$) as well as the SIT coefficient determined for the complex $Ca[Ni(OH)(H_1cit)]^-$ are summarized in Tables 2 and 3, respectively.

Fig. 6(a–h) compares experimental solubility data determined in this work, with solubility calculations using the thermodynamic and activity models summarized in Tables 2 and 3 Thin dashed lines in the figures correspond to the prevailing aqueous species underlying the solubility curves. This comparison confirms the excellent agreement between experimental and model data, for a wide range of boundary conditions, *i.e.*, pH, citrate concentration and ionic strength, as well as in the absence and presence of Ca.

4. Implications for the chemical behaviour of Ni(II) in alkaline systems containing citrate

The new chemical, thermodynamic and SIT activity models derived in this work allow for the first time the calculation of Ni(II) solubility and aqueous speciation in alkaline to hyperalkaline solutions containing citrate. Fig. 7 shows the predominance diagrams of Ni(II) calculated within $9 \le pH \le 13.5$ and $1{\bullet}10^{-5}$ mol $kg^{-1} \le [cit]_{tot} \le 0.03$ mol kg^{-1}, in the absence (Fig. 7a) and presence of Ca (Fig. 7b, with [Ca] = 0.02 mol kg^{-1}). The latter Ca concentration is representative of the pore water in the degradation stage II of cement, as buffered by the equilibrium with portlandite at pH ≈ 12.5 (Ochs et al., 2016; Wieland, 2014).

Fig. 7a confirms the relevant role of Ni(II)-cit complexes in Ca-free, alkaline to hyperalkaline pH conditions, even though the stability of these complexes decreases with increasing pH. Hence, at pH ≈ 10 the binary complex Ni(cit)$^-$ prevails already at [cit] ≈ $2{\bullet}10^{-5}$ mol kg^{-1},

Table 3
Summary of the SIT coefficients for the Ni(II) aqueous complexes considered in this work, as determined in this work or reported in the literature.

i	*k*	ε(*i*,*k*) [kg·mol^{-1}]	Reference
Ni^{2+}	Cl^-	(0.17 ± 0.02)	Gamsjäger et al. (2005)
$NiCl^+$	Cl^-	(0.21 ± 0.06)	(González-Siso et al., 2018)
$Ni(OH)_2$(aq)	Na^+, Ca^{2+}, Cl^-	0	By definition in SIT
Na^+	cit^{3-}	–(0.076 ± 0.030)	Hummel et al. (2005)
Na^+	Ca(cit)$^-$	(0.03 ± 0.03)	Same value as Mg(cit)$^-$, as selected in (Hummel et al., 2005)
Na^+	Ni(cit)$^-$	(0.10 ± 0.20) (0.22 ± 0.5)	This work (Hummel et al., 2005)
Na^+	$Ni(H_1cit)^{2-}$	–(0.04 ± 0.10)	This work
Na^+	$Ni(OH)(H_1cit)^{3-}$	(0.13 ± 0.20)	This work
Na^+	$Ni(cit)_2^{4-}$	(0.15 ± 0.10)	This work
Na^+	$Ni(cit)(H_1cit)^{5-}$	(0.05 ± 0.10)	This work
Na^+	$Ni(H_1cit)_2^{5-}$	–(0.09 ± 0.20)	This work
Na^+	$Ca[Ni(OH)(H_1cit)]^-$	–(0.16 ± 0.10)	This work

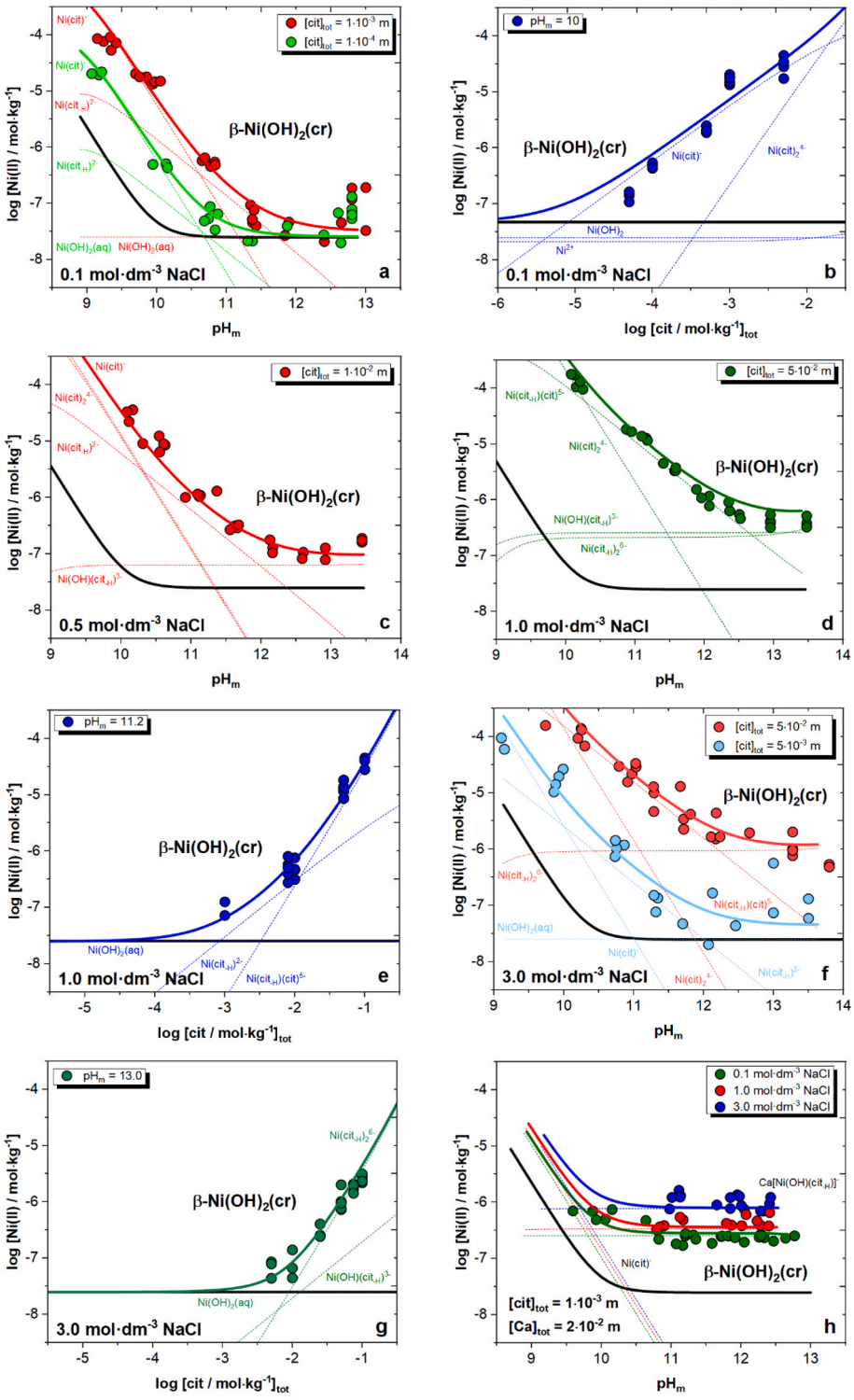

Fig. 6. Comparison of experimental solubility data determined in this work and solubility calculations using the thermodynamic and activity models derived in this work for the system Na^+–Ca^{2+}–Ni^{2+}–Cl^-–OH^-–cit^{3-}–H_2O(l), as summarize in Tables 2 and 3

whereas more than two orders of magnitude higher citrate concentrations are required for the complex $Ni(OH)(H_{-1}cit)^{3-}$ to become predominant at pH ≈ 13. The presence of Ca significantly changes the speciation scheme and the stability of the Ni(II)-cit complexes in hyperalkaline pH conditions (Fig. 7b). Hence, Ca promotes the stabilization of the $Ni(OH)(H_{-1}cit)^{3-}$ moiety at a significantly lower ligand concentration, *i.e.*, [cit] ≈ 10^{-4} mol kg^{-1}. This is expectedly caused by the strong ionic interaction between Ca^{2+} and $Ni(OH)(H_{-1}cit)^{3-}$:

$$Ca^{2+} + Ni(OH)(H_{-1}cit)^{3-} \Leftrightarrow Ca[Ni(OH)(H_{-1}cit)]^- \quad (17)$$

with log $^*K^\circ(17) = (6.3 \pm 0.5)$, calculated combining the complexation constants derived in this work for $Ni(OH)(H_{-1}cit)^{3-}$and $Ca[Ni(OH)(H_{-1}cit)]^-$ (see Table 2).

The stability of the ternary complex Ca–Ni(II)–cit can be also compared with the formation of other ternary complexes triggered by

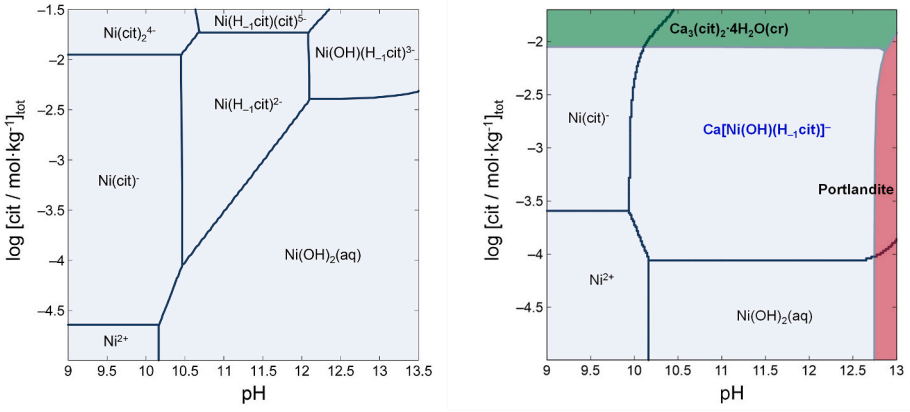

Fig. 7. Predominance diagrams of Ni(II) under varying pH and log [cit], (a) in the absence of Ca, and (b) in the presence of [Ca] = 0.02 mol kg^{-1}. Calculations performed with thermodynamic data reported by González-Siso et al. (solubility and hydrolysis) and determined in this work (Ni(II)–cit system), using the geochemical code Geochemist's Workbench (Bethke, 2022). Calculations conducted for [Ni(II)]$_{tot}$ = 1·10^{-9} mol kg^{-1} and I = 0.5 mol dm^{-3} NaCl–NaOH–Na$_3$cit, except at high citrate concentrations, where deviations in ionic strength occur due to the contribution of the cit^{3-} and Na$^+$ ions. Red and green regions in (b) indicate the precipitation of Ca(OH)$_2$(cr) and Ca$_3$(cit)$_2$•4H$_2$O(cr).

ionic interactions between anionic binary complexes and Ca^{2+}, *e.g.*:

$$Ca^{2+} + Pu(OH)_4(ISA)^- \Leftrightarrow Ca[Pu(OH)_4(ISA)]^+ \quad (18)$$

$$\log {}^*K^\circ(18) = (3.37 \pm 0.16) \text{ (Tasi et al., 2018)}$$

$$Ca^{2+} + Pu(OH)_5(ISA)^{2-} \Leftrightarrow Ca[Pu(OH)_5(ISA)](aq) \quad (19)$$

$$\log {}^*K^\circ(19) = (4.22 \pm 0.15) \text{ (Tasi et al., 2018)}$$

or the well-established formation of the ternary Ca–U(VI)–CO_3 aqueous complexes:

$$Ca^{2+} + UO_2(CO_3)_3^{4-} \Leftrightarrow CaUO_2(CO_3)_3^{2-} \quad (20)$$

$$\log {}^*K^\circ(20) = (5.2 \pm 0.2) \text{ (Grenthe et al., 2020)}$$

These results highlight that, in spite of the very stable aqueous complexes and solid compounds formed by Ca with citrate, the complexation of citrate with Ni(II) is not outcompeted by calcium due to the participation of Ca in the formation of quaternary complexes. Similar observations were recently reported by DiBlasi and co-workers for the Ca–Pu(IV)–EDTA and Ca–Pu(III)–EDTA systems (DiBlasi et al., 2021, 2022; Trumm et al., 2022), notwithstanding the great stability of the binary complex CaEDTA^{2-} ($\log K^\circ_{(1,1)}$ = 12.69 ± 0.06) (Hummel et al., 2005).

As discussed in the introduction and widely reported in the literature, the interaction of cement with groundwater leads to the subsequent dissolution of different cement phases and corresponding evolution of the porewater composition, particularly in terms of pH, [Ca] and [Si]. The non-ideal multisite CASH + solid solution model derived by Kulik, Miron and co-workers provides an accurate description of C–S–H solubility and pore solution composition as a function of pH and alkali concentration (Kulik et al., 2022; Miron et al., 2022a, 2022b). Information on the evolution of [Ca] and [Si] as a function of pH were reported in (Cevirim-Papaioannou et al., 2023) based on model calculations with CASH + (see Fig. 8a). This information has been used in Fig. 8b as input for the calculation of Ni(II) speciation in the presence of citrate along degradation stages I to III of cement. Fig. 8b shows that in the presence of [cit] = 10^{-3} mol kg^{-1}, the quaternary complex Ca[Ni(OH)(H$_{-1}$cit)]$^-$ prevails over a broad range of pH extending from degradation stages I to III. In the later steps of the degradation stage III, the drop in pH together with the decrease in Ca concentration leads to the predominance of Ni(H$_{-1}$cit)$^{2-}$ and, ultimately, Ni(cit)$^-$.

5. Summary and conclusions

The solubility and complexation behaviour of Ni(II) in the presence of citrate was investigated with a comprehensive series of undersaturation solubility experiments with β-Ni(OH)$_2$(cr). Experiments were conducted at T = (22 ± 2)°C under inert gas (Ar) atmosphere, with 9 ≤ pH$_m$ ≤ 13.5, 5•10^{-5} mol kg^{-1} ≤ [cit] ≤ 0.1 mol kg^{-1} and 0.1 M ≤ I ≤ 3.0 mol dm^{-3} NaCl–NaOH–Na$_3$cit solutions, both in the absence and presence of 0.02 mol kg^{-1} $CaCl_2$.

Solid phase characterization by XRD confirmed that β–Ni(OH)$_2$(cr) is the solid phase controlling the solubility in all investigated systems containing citrate. In systems containing citrate and Ca, the absence of any features corresponding to either Ca$_3$Cit$_2$·4H$_2$O(cr) or Ca(OH)$_2$(cr) is in line with thermodynamic calculations, which predict undersaturation conditions with respect to both solid phases within the investigated boundary conditions.

Citrate promotes a clear enhancement in the solubility of Ni(II) with respect to ligand-free systems, thus indicating the formation of Ni(II)–cit aqueous complexes. Thermodynamic calculations using the current NEA-TDB selection clearly underestimate the solubility of Ni(II) in the alkaline to hyperalkaline pH$_m$ conditions of relevance in cementitious systems with presence of citrate. Such discrepancy is explained by the formation of additional complexes not included in the present NEA-TDB selection. Taking as anchoring point the species Ni(cit)$^-$ and Ni(cit)$_2^{4-}$, currently selected in the NEA-TDB, and based on slope analysis of solubility data ($\log_{10}$ [Ni] *vs.* pH$_m$ and $\log_{10}$ [Ni] *vs.* $\log_{10}$ [cit]), the predominance of the complexes Ni(H$_{-1}$cit)$^{2-}$, Ni(OH)(H$_{-1}$cit)$^{3-}$, Ni(cit)(H$_{-1}$cit)$^{5-}$ and Ni(H$_{-1}$cit)$_2^{6-}$ at pH$_m$ ≥ 10 is proposed, with H$_{-1}$cit corresponding to a citrate ligand with deprotonated alcohol group. In Ca-containing systems, the predominance of the complex Ca(cit)$^-$ significantly decreases the concentration of free ligand in the aqueous phase. Accordingly, the increase in the solubility of Ni(II) observed in the presence of citrate and Ca can only be explained claiming the formation of a ternary or quaternary complex involving the participation of Ca. The best fit of solubility data was obtained considering the formation of the complex Ca[Ni(OH)(H$_{-1}$cit)]$^-$, although the formation of other complexes with a different stochiometric numbers of citrate and/or Ca cannot be disregarded under experimental conditions beyond those considered in this work.

The chemical, thermodynamic and SIT activity models derived in this work for the system Na$^+$–Ca^{2+}–Ni^{2+}–Cl$^-$–OH$^-$–cit^{3-}–H$_2$O(l) can be implemented in thermodynamic databases and geochemical calculations of relevance in the context of nuclear waste disposal. In cementitious systems, scoping calculations emphasize the relevance of the quaternary complex Ca[Ni(OH)(H$_{-1}$cit)]$^-$, particularly in the degradation stage II of cement, but also in the degradation stage I, and III at pH$_m$

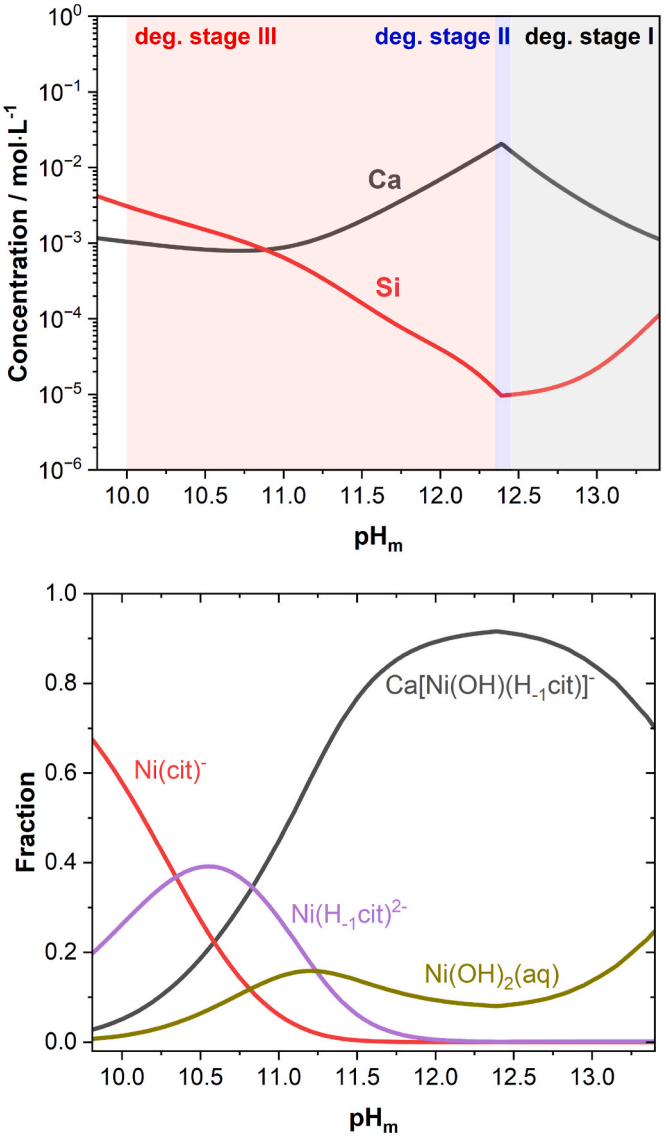

Fig. 8. (a) Evolution pore solution composition as a function of pH during the process of cement degradation, as calculated in (Cevirim-Papaioannou et al., 2023) with the CASH + model; (b) Fraction diagram of Ni(II) in the presence of $[cit]_{tot} = 1 \bullet 10^{-3}$ mol kg^{-1} within $9.7 \leq pH_m \leq 13.7$ for the pore water composition shown in (a), as calculated using the thermodynamic and activity models derived in this work for the system Na^+–Ca^{2+}–Ni^{2+}–Cl^-–OH^-–cit–H_2O (l). Calculations performed using the chemical equilibrium code Spana (Puigdomenech et al., 2014).

values above ~ 11.

CRediT authorship contribution statement

O. Almendros-Ginestà: Writing – review & editing, Writing – original draft, Validation, Methodology, Investigation, Formal analysis, Data curation, Conceptualization. **S. Duckworth:** Writing – review & editing, Validation, Supervision, Project administration, Data curation. **P.Q. Fürst:** Software, Investigation, Formal analysis. **T. Missana:** Writing – review & editing, Validation, Funding acquisition. **M. Altmaier:** Writing – review & editing, Validation. **X. Gaona:** Writing – review & editing, Visualization, Validation, Supervision, Software, Resources, Project administration, Funding acquisition, Data curation, Conceptualization.

Declaration of competing interest

The authors declare that they have no known competing financial interests or personal relationships that could have appeared to influence the work reported in this paper.

Acknowledgment

The EURAD project leading to this application has received funding from the European Union's Horizon 2020 research and innovation programme under grant agreement No 847593, as part of the Work Package CORI, Cement-Organic-Radionuclide-Interaction. This work was partially funded by the R + D Spanish national plan ARNO (PID2019-106398 GB-I00) and the ENEN2plus project (HORIZON-EURATOM-2021-NRT-01-13 101061677), funded by the European Union.

Appendix A. Supplementary data

Supplementary data to this article can be found online at https://doi.org/10.1016/j.apgeochem.2025.106290.

Data availability

Data will be made available on request.

References

Adam, N., Hinz, K., Gaona, X., Panak, P.J., Altmaier, M., 2021. Impact of selected cement additives and model compounds on the solubility of Nd(III), Th(IV) and U(VI): screening experiments in alkaline NaCl, $MgCl_2$ and $CaCl_2$ solutions at elevated ionic strength. Radiochim. Acta (accepted).

Altmaier, M., Metz, V., Neck, V., Müller, R., Fanghänel, T., 2003. Solid-liquid equilibria of $Mg(OH)_2$(cr) and $Mg_2(OH)_3Cl\ 4H_2O$(cr) in the system Mg-Na-H-OH-O-Cl-H_2O at 25°C. Geochim. Cosmochim. Acta 67, 3595–3601.

Bethke, C.M., 2022. Geochemical and Biogeochemical Reaction Modeling, third ed. Cambridge University Press, Cambridge.

Borkowski, M., Choppin, G.R., Moore, R.C., Free, S.J., 2000. Thermodynamic modeling of metal-ligand interactions in high ionic strength NaCl solutions:: the Co-citrate and Ni-citrate systems. Inorg. Chim. Acta. 298, 141–145.

Cevirim-Papaioannou, N., Androniuk, I., Miron, G.D., Altmaier, M., Gaona, X., 2023. Beryllium solubility and hydrolysis in dilute to concentrated $CaCl_2$ solutions: thermodynamic description in cementitious systems. Frontiers in Nuclear Engineering 2, 1192463.

Ciavatta, L., 1980. The specific interaction theory in evaluating ionic equilibria. Ann. Chim-Rome 70, 551–567.

Daniele, P.G., Ostacoli, G., Rigano, C., Sammartano, S., 1984. Ionic-strength dependence of formation-constants .4. Potentiometric study of the system Cu-2+-Ni-2+-Citrate. Transit Metal Chem 9, 385–390.

Daniele, P.G., Ostacoli, G., Zerbinati, O., Sammartano, S., Derobertis, A., 1988. Mixed metal-complexes in solution - thermodynamic and spectrophotometric study of copper(II)-citrate heterobinuclear complexes with nickel(II), zinc(II) or cadmium(II) in aqueous-solution. Transit Metal Chem 13, 87–91.

DiBlasi, N.A., Dardenne, K., Prüssmann, T., Duckworth, S., Altmaier, M., Gaona, X., 2023. Technetium complexation with multidentate carboxylate-containing ligands: trends in redox and solubility phenomena. Environ. Sci. Technol. 57, 3661–3670.

DiBlasi, N.A., Tasi, A.G., Gaona, X., Fellhauer, D., Dardenne, K., Rothe, J., Reed, D.T., Hixon, A.E., Altmaier, M., 2021. Impact of Ca(II) on the aqueous speciation, redox behavior, and environmental mobility of Pu(IV) in the presence of EDTA. Sci. Total Environ. 783.

DiBlasi, N.A., Tasi, A.G., Trumm, M., Schnurr, A., Gaona, X., Fellhauer, D., Dardenne, K., Rothe, J., Reed, D.T., Hixon, A.E., Altmaier, M., 2022. Pu(iii) and Cm(iii) in the presence of EDTA: aqueous speciation, redox behavior, and the impact of Ca(ii). Rsc Adv 12, 9478–9493.

Duro, L., Domenech, C., Grive, M., Roman-Ross, G., Bruno, J., Kallstrom, K., 2014. Assessment of the evolution of the redox conditions in a low and intermediate level nuclear waste repository (SFR1, Sweden). Appl. Geochem. 49, 192–205.

Duro, L., Grive, M., Gaona, X., Bruno, J., Andersson, T., Boren, H., Dario, M., Allard, B., Hagberg, J., Källström, K., 2012. Study of the effect of the fibre mass UP2 degradation products on radionuclide mobilisation. SKB R-12-15.

Felipe-Sotelo, M., Edgar, M., Beattie, T., Warwick, P., Evans, N.D.M., Read, D., 2015. Effect of anthropogenic organic complexants on the solubility of Ni, Th, U(IV) and U (VI). J. Hazard Mater. 300, 553–560.

Felmy, A.R., Cho, H., Dixon, D.A., Xia, Y.X., Hess, N.J., Wang, Z.M., 2006. The aqueous complexation of thorium with citrate under neutral to basic conditions. Radiochim. Acta 94, 205–212.

Gamsjäger, H., Bugajski, J., Gajda, T., Lemire, R., Preis, W., 2005. Chemical Thermodynamics Vol. 6. Chemical Thermodynamics of Nickel. Elsevier, North Holland, Amsterdam.
Giffaut, E., Grive, M., Blanc, P., Vieillard, P., Colas, E., Gailhanou, H., Gaboreau, S., Marty, N., Made, B., Duro, L., 2014. Andra thermodynamic database for performance assessment: ThermoChimie. Appl. Geochem. 49, 225–236.
González-Siso, M.R., Gaona, X., Duro, L., Altmaier, M., Bruno, J., 2018. Thermodynamic model of Ni(II) solubility, hydrolysis and complex formation with ISA. Radiochim. Acta 106, 31–45.
Grenthe, I., Gaona, X., Plyasunov, A.V., Rao, L., Runde, W.H., Grambow, B., Konings, R.J. M., Smith, A.L., Moore, E.E., 2020. Second update on the chemical thermodynymics of uranium, neptunium, plutonium, americium and technetium. In: Nuclear Energy Agency of the OECD (NEA), vol. 14.
Guidone, R.E., Gaona, X., Winnefeld, F., Altmaier, M., Geckeis, H., Lothenbach, B., 2024. Citrate sorption on cement hydrates. Cement Concr. Compos. 178, 107404.
Hedwig, G.R., Liddle, J.R., Reeves, R.D., 1980. Complex formation of nickel(II) ions with citric acid in aqueous solution - a potentiometric and spectroscopic study. Aust. J. Chem. 33, 1685–1693.
Heitner-Wirguin, C., Friedman, D., Goldschmidt, J.M.E., Shamir, J., 1958. r. Contribution à l'etude des complexes des citrates et tartrates. 3. Le complexe du nickel avec le citrate. B. Soc. Chim. F 864–867.
Hummel, W., Anderegg, G., Rao, L., Puigdomènech, I., Tochiyama, O., 2005. Chemical Thermodynamics Vol. 9. Chemical Thermodynamics of Compounds and Complexes of U, Np, Pu, Am, Tc, Se, Ni and Zr with Selected Organic Ligands. Elsevier, North Holland, Amsterdam.
Hummel, W., Thoenen, T., 2023. The PSI chemical thermodynamic database 2020. Nagra Technical Report 21-03.
Keith-Roach, M., Lindgren, M., Källström, K., 2021. Assessment of complexing agent concentrations for the post-closure safety assessment in PSAR SFR. SKB R-20-04.
Keith-Roach, M., Shahkarami, P., 2021. Organic materials with the potential for complexation in SFR, the final repository for short-lived radioactive waste. SKB R-21-03.
Kitamura, A., 2021. JAEA-TDB-RN in 2020: update of JAEA's thermodynamic database for solubility. Speciation of Radionuclides for Performance Assessment of Geological Disposal of High-Level and TRU Wastes. JAEA-Data/Code 2020-020.
Kulik, D.A., Miron, G.D., Lothenbach, B., 2022. A structurally-consistent CASH + sublattice solid solution model for fully hydrated C-S-H phases: thermodynamic basis, methods, and Ca-Si-H_2O core sub-model. Cement Concrete Res 151.
Lindgren, M., Pettersson, M., Wiborgh, M., 2007. Correlation factors for C-14, Cl-36, Ni-59, Ni-63, Mo-93, Tc-99, I-129 and Cs-135. SKB Rapport R-07-05.
Migal, P.K., Sychev, A.Y., 1958. Stability of citric acid complexes of some metals. Russ J Inorg Chem+ 3, 104–117.
Miron, G.D., Kulik, D.A., Lothenbach, B., 2022a. Porewater compositions of Portland cement with and without silica fume calculated using the fine-tuned CASH plus NK solid solution model. Mater. Struct. 55.
Miron, G.D., Kulik, D.A., Yan, Y.R., Tits, J., Lothenbach, B., 2022b. Extensions of CASH + thermodynamic solid solution model for the uptake of alkali metals and alkaline earth metals in C-S-H. Cement Concrete Res 152.
Möschner, G., Lothenbach, B., Figi, R., Kretzschmar, R., 2009. Influence of citric acid on the hydration of Portland cement. Cement Concrete Res 39, 275–282.
Ochs, M., Dolder, F., Tachi, Y., 2022. Decrease of radionuclide sorption in hydrated cement systems by organic ligands: comparative evaluation using experimental data and thermodynamic calculations for ISA/EDTA-actinide-cement systems. Appl. Geochem. 136.
Ochs, M., Mallants, D., Wang, L., 2016. Radionuclide and metal sorption on cement and concrete. Topics in Safety, Risk, Reliability and Quality, first ed. Springer International Publishing: Imprint: Springer, Cham, p. 1. online resource (XXX, 301 pages).
Palmer, D.A., Gamsjäger, H., 2010. Solubility measurements of crystalline β-$Ni(OH)_2$ in aqueous solution as a function of temperature and pH. J. Coord. Chem. 63, 2888–2908.
Patnaik, R.K., Pani, S., 1957. Citrate complex of nickel. J. Indian Chem. Soc. 34, 619–628.
Patnaik, R.K., Pani, S., 1965. Studies on the citrate complex of nickel by solubility, pH-titraton and conductimetric titration methods. J. Indian Chem. Soc. 42, 793–798.
Puigdomenech, I., Colàs, E., Grivé, M., Campos, I., García, D., 2014. A tool to draw chemica equilibrium diagrams using SIT: applications to geochemical systems and radionuclide solubility. In: Duro, L., Giménez, J., Casas, I., de Pablo, J. (Eds.), Scientific Basis for Nuclear Waste Management XXXVII. Materials Research Society.
Salnikov, Y.I., Devyatov, F.V., Zhuravleva, N.E., Golodnitskaya, D.V., 1984. Complex formation of nickel(II) and cobalt(II) with citric acid. Zh Neorg Khim+ 29, 2273–2276.
Sari, H., 2001. Determination of stability constants of citrate complexes with divalent metal ions (M2+ = Mg, ca, Ni, Cu and Zn) in aqueous solutons. Energy Educ. Sci. Technol. 6, 85–103.
Szabo, P.G., Tasi, A.G., Gaona, X., Maier, A.C., Hedström, S., Altmaier, M., Geckeis, H., 2023. Impact of the degradation leachate of the polyacrylonitrile-based material UP2W on the retention of Ni(II), Eu(III) and Pu(IV) by cement. Dalton T 52, 13324–13331.
Tasi, A., Gaona, X., Fellhauer, D., Böttle, M., Rothe, J., Dardenne, K., Polly, R., Grivé, M., Colas, E., Bruno, J., Källström, K., Altmaier, M., Geckeis, H., 2018. Thermodynamic description of the plutonium - alpha-D-isosaccharinic acid system II: formation of quaternary Ca(II)-Pu(IV)-OH-ISA complexes. Appl. Geochem. 98, 351–366.
Tasi, A., Szabo, P., Gaona, X., Bouby, M., Sittel, T., Schild, D., Maier, A.C., Hedström, S., Altmaier, M., Geckeis, H., 2024. Degradation of the polyacrylonitrile-based UP2W material under cementitious conditions. Appl. Geochem. 169.
Taylor, H.F.W., 1997. Cement Chemistry, second ed. T. Telford, London.
Trumm, M., Tasi, A., Schnurr, A., DiBlasi, N.A., Gaona, X., 2022. Structural characterisation of hydrolysed Cm(III)-EDTA solution species under alkaline conditions: a TRLFS, vibronic side-band and quantum chemical study. Mol. Phys. 120.
Wieland, E., 2014. Sorption data base for the cementitious near field of L/ILW and ILW repositories for provisiona safety analyses for SGT-E2. Nagra Technical Report 14-08.